Chalcogenide Letters Vol. 21, No. 12, December 2024, p. 1001 - 1009

Probing $SnSO_3/ZnSO_3$ nanocomposites by optical and magnetic perspective

R. Gayathri [a], S. Shanmugha Soundare [b], K. Haritha [a], S. Ariponnammal [a,*]
[a] *Department of Physics, Gandhigram Rural Institute, Deemed To Be University, Gandhigram-624302, Dindigul District, Tamilnadu, India*
[b] *Centre for Nanoscience and Technology, Anna University, Chennai-600025, Tamilnadu, India*

$SnSO_3/ZnSO_3$ nanocomposite has been synthesized using the hydrothermal process. The complete formation of the $SnSO_3/ZnSO_3$ nanocomposite is confirmed by XRD and EDAX. It displays a fascinating rectangular bar shape. The measured particle size is 100.4 nm. It will be a promising option for optoelectronic devices. Energy gap of the $SnSO_3/ZnSO_3$ nanocomposite is 5.85 eV. The refractive index of the nanocomposite through its energy gap is found to be 1.883. The ultraviolet (~387.2 nm) area of the PL emission spectrum exhibits the strong efficient emission, while the green (~522.1 nm) region and the red (~789.4 nm) region show weak and moderate emission, respectively. Radiative electron-hole recombination is seen in the UV emission at 387.2 nm, which qualifies the contender for displays/projection-based applications. Emission peaks observed in the visible region is attributed to various defects Frenkel or Schottky defects, Tin or Zinc interstitials and oxygen vacancies. The finger print region's S-O, Zn-O, and Sn-O bands are confirmed by the accurately assigned FTIR bands. At 300K, the sample displays diamagnetic behaviour. Additionally, at 5K, it displays an intriguing super paramagnetic behaviour between -0.15 Tesla and 0.15 Tesla.

(Received October 7, 2024; Accepted December 6, 2024)

Keywords: $SnSO_3/ZnSO_3$ nanocomposite, Hydrothermal method, Structural, Optical, Magnetic studies

1. Introduction

Oxychalcogenides are notable compounds of mixed anions, wherein one or more cations are indirectly bonded to both the oxide anion and the chalcogen (S, Se, Te) anions, forming an arrangement of oxide and chalcogen layers alternatively. The oxychalcogenide, mixed anion compounds typically demonstrate more favourable results in their physical, thermal, optical, electrical, and electronic properties when combined with transition, post-transition, or rare earth metals [1]. Metal oxychalcogenides can be synthesized using various methods such as hydrothermal synthesis, sol-gel technique, chemical deposition method, Laser treated ablation method, sono chemical method and etc [2]. Regarding its particle size and the structural arrangement of atoms in the lattice plane, which significantly influences the compound's physical properties, the produced chemical offers a variety of uses. The compound can be either insulating, conducting, or semi-conducting based on its improved and modified physical properties, which essentially depend on the elements that make up the compound [3]. The attractive results of the metal oxychalcogenides give its pathway in numerous technological applications especially in overviewing optoelectronics and thermoelectric. Metal oxychalcogenides have peculiar optical properties such as transparent semiconducting behavior and wider band gap range. Hence in some special case, oxychalcogenides act as wider band gap semiconductor rather than insulator [4]. These wider band gap semiconductors have customizable electrical conductivity, controlled carrier concentration, and excellent optical transparency, making them indispensable for fabricating new electronic devices. The most efficiently investigated transparent conductive oxides comes under wider band gap semiconductor,

* Corresponding author: ariponnammal@gmail.com
https://doi.org/10.15251/CL.2024.2112.1001

which are applied in the fabrication of displays and solar cells, power electronics and also in various opto-electronic devices [5]. The nanocomposite materials are used in solar cells as the window layer and transparent conducting electrode (TCE), since they have a broader band gap range and greater electrical conductivity both necessary to capture the solar radiative spectrum [6].

Metal oxychalcogenides give interesting response when it is allowed to be interacted with the external magnetic field. Certain compounds show very different magnetic response below its regular temperature, which provides new idea of studying the low temperature response of the compound in order to find the notable change in its behavior. Some of the oxychalcogenide compounds show peculiar change in its ferromagnetic/ antiferromagnetic behavior due to its surface inhomogeneities such as defects and patterns in its crystal plane [7]. In recent times, many studies have been conducted on some oxychalcogenides as potential thermoelectric materials. These materials exhibit a variety of intriguing electrical characteristics due to the presence of ionic oxide with alternate covalent chalcogenide layers. Additionally, the materials allow characteristics to be tuned by substituting chemicals at the coexisting layer [8]. As efficient thermoelectric materials, oxychalcogenides offer guidance for possible uses involving thermal energy to electrical energy conversion and the opposite. The development of such oxychalcogenide compounds in thermo electrical application is possible with the higher understanding of their composition, crystal structure, defects and bonding nature [9]. To summarize, oxychalcogenides are diverse family of materials possessing a multitude of characteristics and uses [10]. Their unique blend of chalcogen and oxygen components allows them to suit a variety of technical demands. This work investigates the $SnSO_3/ZnSO_3$ oxychalcogenide nanocomposite.

2. Methods and materials

The nanocomposite $SnSO_3/ZnSO_3$ was synthesized using the hydrothermal process. Alfa Aesar analytical grade chemicals ($ZnCl_3$, $SnCl_3$, and Na_2SO_3) are taken and 0.1 M of each chemical is prepared by dissolving it in 30 ml of double-distilled water separately. Freshly prepared aqueous 0.1M Na_2SO_3 solution was combined drop by drop with the mixture solution of 0.1M $ZnCl_3$ and 0.1M $SnCl_3$, which is constantly stirred at 400 rpm. After that, entire solution is placed in a Teflon container and autoclaved for approximately eight hours at a steady 60°C. A precipitate of grey-white coloured was produced after cooling. It is undergone centrifuging process once it has done many washings, initially with double-distilled water and then with ethanol. After a few hours of drying at 50 °C, the precipitate was put in a desiccator.

The Energy dispersive X-ray analysis spectrum (EDAX) is recorded using the model OXFORD INCAPENTAx3. Using Cu Kα radiation, Panalytical X'Pert Pro records scanning electron microscopy (SEM) and also X-ray powder diffraction (XRD) using the Carel ZEISS EVO-18 model. The ultraviolet-visible (UV-Vis) spectrum is obtained using the Perkin Elmer Lambda 35 spectrophotometer. The photoluminescence (PL) spectrum is obtained using the VARIAN Cary Eclipse Fluorescence Spectrophotometer. The Fourier transform infrared (FTIR) spectrum is obtained using the Perkin Elmer BX model spectrophotometer and the Lakeshore model VSM 7410 is utilized for magnetic measurements.

3. Results and discussions

3.1. Morphological studies

The EDAX result of $SnSO_3/ZnSO_3$ nanocomposite sample is shown in Figure 1. Existence of Sn, Zn, S and O components in the sample is detected, indicating the purity of the product. Tin, zinc, sulphur, and oxygen weight percentages are 38.20%, 2.11%, 2.06%, and 57.63% have been detected respectively. The analysis verifies that the $SnSO_3/ZnSO_3$ nanocomposite formed perfectly. SEM image of $SnSO_3/ZnSO_3$ at 35 KX magnification (Figure 2) displays a rectangular bar with an attractive shape. Using the particle size analyser, the particle is observed to be 100.4 nm in size.

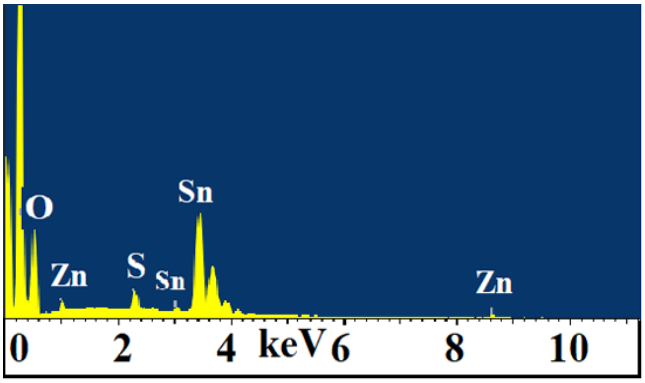

Fig. 1. EDAX of $SnSO_3/ZnSO_3$ nanocomposite.

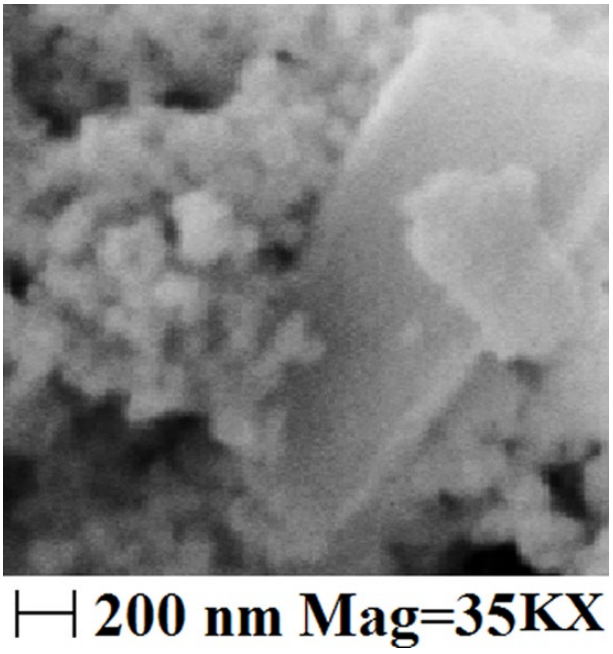

Fig. 2. SEM picture of $SnSO_3/ZnSO_3$ Nanocomposite.

3.2. XRD

Figure 3 depicts the XRD pattern of $SnSO_3/ZnSO_3$ nanocomposite. The structure of synthesized nanocomposite was analysed and is noticed that the $SnSO_3$ exhibits high intensity peaks with the 2θ values 30.4825, 31.6724, 33.598, 44.5997 and 45.5625, which are indexed with the respective planes of (002), (10$\bar{2}$), ($\bar{1}\bar{1}\bar{1}$), ($\bar{2}$02) and ($\bar{2}\bar{1}$0) with monoclinic structure along with a = 4.474 Å, b = 5.295 Å, and c = 6.266 Å lattice parameters [11]. For $ZnSO_3$, 2θ values are found at 26.6096, 37.6114, 39.0934, 51.2635, 61.3565, 64.2232 and 65.4673, which are efficiently indexed in the respective planes of ($\bar{1}$11), ($\bar{1}\bar{3}$0), (13$\bar{1}$), (12$\bar{3}$), (203), (22$\bar{3}$) and ($\bar{3}$01) at monoclinic structure along with a = 4.32 Å, b = 8.622 Å, and c = 6.44 Å lattice parameters [12]. Moreover, the missing of certain alloy peaks and lacking of few peak transformations confirm the complete entity of $SnSO_3/ZnSO_3$ nanocomposite [13].

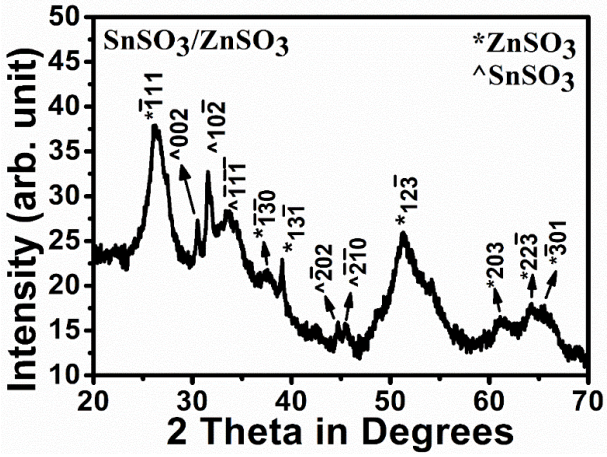

Fig. 3. XRD of $SnSO_3/ZnSO_3$ nanocomposite.

3.3. Optical studies

The UV-VIS absorbance spectrum is recorded and is depicted in Figure 4. Its strong absorption at around 209.95 nm meets the requirements for employing it as a UV filter purpose. The four divisions of ultraviolet radiation are: visible UV (400-800 nm), extremely far UV (200-280 nm), nearer UV (280-400 nm), and vacuum UV (10-200 nm). Among all, visible UV zone has the longest wavelength and the lowest energy, whereas the vacuum UV region has the highest energy. From the Figure 4, it is noted that the $SnSO_3/ZnSO_3$ nanocomposite absorbs the incident light only in the vacuum UV range. This indicates that the electrons in the $SnSO_3/ZnSO_3$ nanocomposite sample have a very high optical energy gap range, and only the incident light with very high energy can excite them [14].

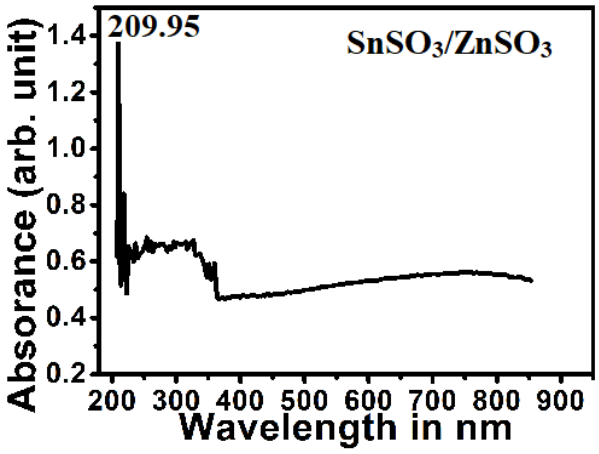

Fig. 4. UV absorbance spectrum of $SnSO_3/ZnSO_3$ nanocomposite.

Lower energy UV light apart from vacuum UV clearly passes through $SnSO_3/ZnSO_3$ samples unabsorbed since their energy is insufficient to close the energy gap. A tiny absorption in the sample's visible range indicates the molecules or chromophores present is of lower concentration. When permitted to interact with incident light, the attached double bonds or aromatic rings that constitute chromophores can alter electrically. According to the Beer-Lambert law, which states that the amount of light absorbed by a sample is proportionate to the concentration of chromophores [14-16]. Consequently, a lower absorption indicates a strong light transmission through the material or a low concentration of chromophores. On the other hand, a small absorption may indicate a short path length in the sample or lower molar absorptivity of chromophores [14-16].

These components significantly distract sample's absorbance range, as defined in the equation of Absorbance (A),

$$A = \epsilon cl \tag{1}$$

where, ϵ is molar absorptivity constant, c is concentration of the sample, and l is path length [14]. Because of presence of fewer chromophores in the visible spectrum, higher transmittance is thus observed. Figure 5 shows the spectrum of UV-visible reflectance. The $SnSO_3/ZnSO_3$ nanocomposite exhibits broad transmission from 364 to 900 nm and broad reflectance in the same range, rendering a promising behaviour for optoelectronic devices.

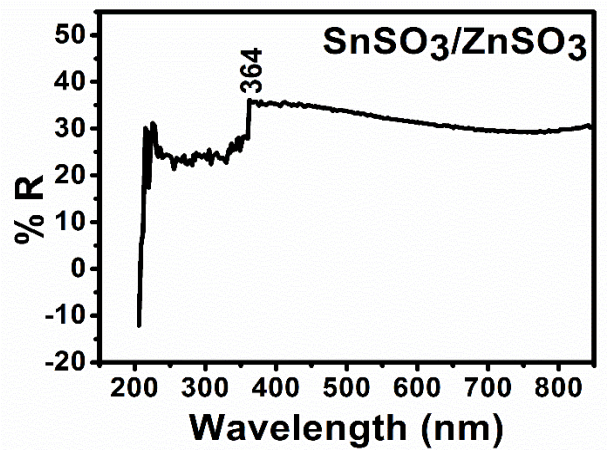

Fig. 5. UV Reflectance of $SnSO_3/ZnSO_3$ nanocomposite.

A taue plot describing energy along x-axis and $(\alpha h\upsilon)^2$ along y-axis, which is depicted in the Figure 6. It is observed from the plot, that an energy gap of $SnSO_3/ZnSO_3$ nanocomposite is 5.85 eV [17-18]. The refractive index (n) of the synthesized nanocomposite is derived as 1.883 using the energy gap (E_{opt}) from relation (2) [19–20],

$$\frac{n^2-1}{n^2+2} = 1-\sqrt{\frac{E_{opt}}{20}} \tag{2}$$

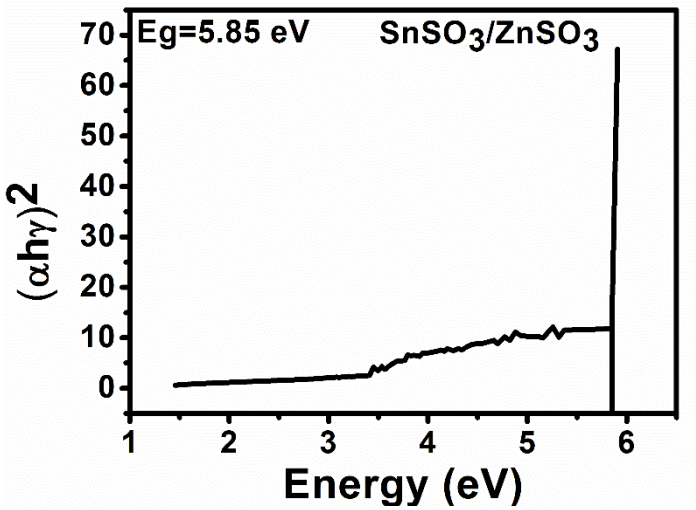

Fig. 6. Taue plot of $SnSO_3/ZnSO_3$ nanocomposite.

PL emission spectrum obtained at an excitation wavelength of 520 nm, which is shown in Figure 7. It displays mild green emission (~522.1 nm), moderate red emission (~789.4 nm), and considerable effective emission in the UV (~387.2 nm) area. The UV region peak at 387.2 nm, is caused due to the envelope of phonon replicas of free exciton luminescence as reported in ZnO [21]. It might be due to the extent of the radiative recombination of electrons and holes. Due to deep peak occurrence in ultraviolet region, it functions as a possible candidate for projection/displays based applications [22]. Emission peak in the visible range is caused due to schottky and frenkel surface defects.

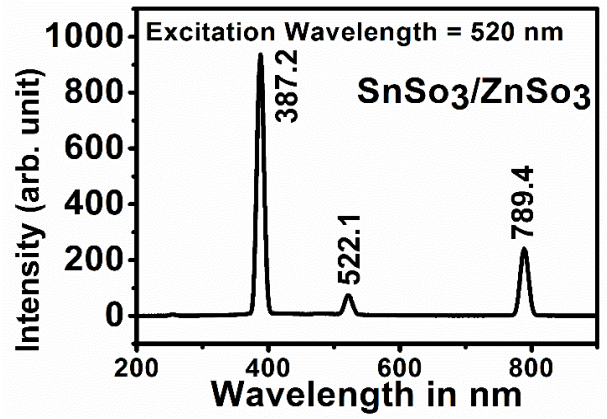

Fig. 7. PL spectrum of $SnSO_3/ZnSO_3$ nanocomposite.

Oxygen lattice vacancies and interstitial spaces are frequently in oxide systems, and their existence has a substantial impact on the photoluminescence response [23–27]. At 522.1 nm, a minor intensity peak is attributed to Zn or Sn interstitials and oxygen vacancies. At 789.4 nm, the medium intensity peak is observed and corresponds to Sn-interstitial defects [28]. These effective results conveys nanocomposites can be employed as ultraviolet photo-conductive detectors, luminescence detectors and optoelectronic devices [26].

3.4. FTIR study

FTIR spectrum of $SnSO_3/ZnSO_3$ nanocomposite is shown in Figure 8. The graph spans broad trough between 3682.9 and 2538.8 cm^{-1} and the O-H bond encloses a peak centred at 3417.9 cm^{-1}[29–31]. Moreover, the bands seen at 2461.2, 1627.2, and 1404.2 are attributed to O-H bonds [29–31]. These results have given hints about the material's hygroscopic properties. Additionally, 1141.9 and 1041.6 cm^{-1} S-O bonds are noted [32]. The bands that make up fingerprint region are corresponding to Sn-O bond at 601.8 cm^{-1} [33] and Zn-O bond at 918.1 cm^{-1} [34-35].

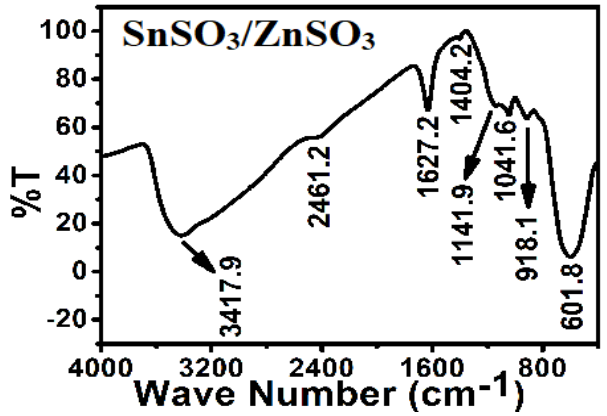

Fig. 8. FTIR spectrum of $SnSO_3/ZnSO_3$ nanocomposite.

3.5. Low temperature magnetic studies

Figure 9 reports the M-H curve analysis of $SnSO_3/ZnSO_3$ nanocomposite proving the diamagnetic nature at 300K [21] and Figure 10 shows the super paramagnetic nature of the synthesized compound at 5K, occurring between the range of -0.15T and 0.15T. The sample shows diamagnetic to super paramagnetic transition with respect to decrease of temperature.

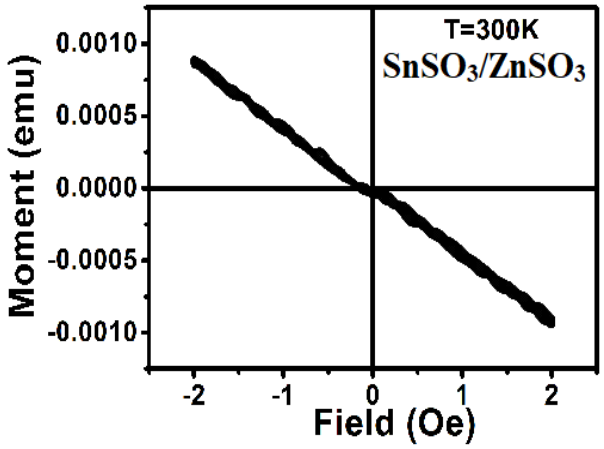

Fig. 9. M-H curve of $SnSO_3/ZnSO_3$ nanocomposite at 300 K.

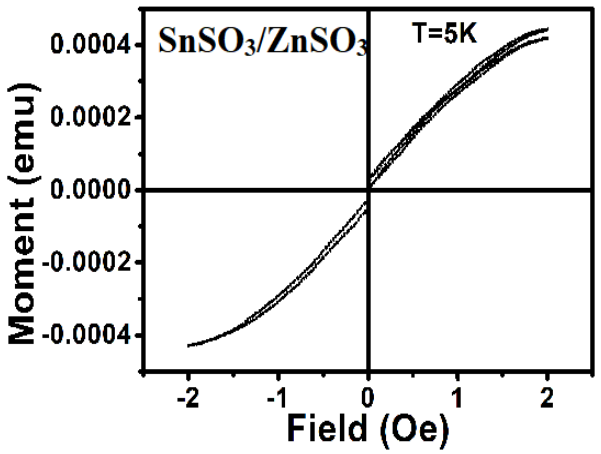

Fig. 10. M-H curve of $SnSO_3/ZnSO_3$ nanocomposite at 5K.

4. Conclusions

On the whole, the hydrothermal technique was used to synthesize the nanocomposite $SnSO_3/ZnSO_3$. EDAX findings for the synthesized nanocomposite $SnSO_3/ZnSO_3$ demonstrate that it is composed of Tin, Zinc, Sulphur and Oxygen, confirming the flawless synthesis and purity of the $SnSO_3/ZnSO_3$ nanocomposite. The SEM results show an intriguing shape of a rectangular bar. The particle size is 100.4 nm. The XRD revealed the complete synthesis of $SnSO_3/ZnSO_3$ through the analysis of presence of peaks with their corresponding hkl planes. It is a suitable option for optoelectronic applications, which has its energy gap of 5.85 eV and the refractive index of 1.883. The PL emission spectrum shows strong efficient emission in the ultraviolet region (~387.2 nm), weak emission in the green visible region (~522.1 nm), and mild emission in the red visible region (~789.4 nm).

Radiative electron-hole recombination may be the reason for the notable rise in the UV area at 387.2 nm, making this possibility an excellent choice for projection and display applications. The emission peaks in visible region in the PL spectra are attributable to various surface defects and interstitial defects in the lattice plane. Oxychalcogenide nanocomposites have the potential to be utilized in optoelectronic device fabrication because of its tunable properties. The FTIR bands are accurately attributed, confirming Sulphur-Oxygen, Zinc-Oxygen, and Tin-Oxygen bonds in the finger print zone. The material being studied is diamagnetic at 300K and paramagnetic at 5K, ranging from -0.15T to 0.15T confirming dia to super paramagnetic transition.

Acknowledgments

Authors express their gratitude to Alagappa University, Karaikudi, Tamilnadu, India's University Science Instrumentation Centre, for providing access to the low temperature magnetic facilities and DST-FIST, Department of Physics, Gandhigram Rural Institute, Deemed To Be University, Gandhigram-624302, Dindigul District, Tamilnadu, India for providing XRD facility.

References

[1]Son D.N. Luu, Paz Vaqueiro, Journal of Materiomics **2**, 131 (2016); https://doi.org/10.1016/j.jmat.2016.04.002
[2] J.C. Lacroix, K.K. Kanazawa, A. Diaz, J. Electrochem. Soc. **136**,1308 (1989); https://doi.org/10.1149/1.2096912
[3] H. Hiramatsu, H. Yanagi, T.Kamiya, K.Ueda, M.Hirano, H. Hosono, Chem. of Mater. **20**, 326 (2008); https://dx.doi.org/10.1021/cm702303r
[4] Shibghatullah Muhammady, Yudhi Kurniawan, Seiya Ishiwata, Awabaikeli Rousuli, Toshiki Nagasaki, Shogo Nakamura, Hitoshi Sato, Atsushi Higashiya,Atsushi Yamasaki, Yoshiaki Hara, Andrivo Rusydi, Kouichi Takase and Yudi dharma, Inorganic Chemistry **57**, 10214 (2018); https://doi.org/10.1021/acs.inorgchem.8b01396
[5] Rachel Woods- Robinson,Yanbing Han, Hanyu Zhang, Tursun Ablekim, Imran Khan, Kristin A. Persson, Andiy Zakutayev, Chem. Rev. **120**, 4007 (2020); https://doi.org/10.1021/acs.chemrev.9b00600
[6] G.Brunin, F.Ricci, V.A.Ha, R.Gian-Marco, H.Geoffroy, npj Comput. Mater. **63**, 5 (2019); https://doi.org/10.1038/s41524-019-0200-5
[7] Y. L. Huang, W.Chen, A. T. S.Wee, Smart Mat. **2**, 139 (2021); doi:10.1002/smm2.1031
[8] A. Parida, S. Senapati, R. Naik, Mater. Today Chem. **26**, 101149 (2022); https://doi.org/10.1016/j.mtchem.2022.101149
[9] Philip Yox, Gayatri Viswanathan, Arka Sarkar, Jian Wang, Kirill Kovnir, Comprehensive Inorganic Chemistry III, **5** (2023); https://doi.org/10.1016/B978-0-12-823144-9.00109-6
[10] Melissa Orr, Glen R. Hebberd, Emma E. McCabe, Robin T. Macaluso, ACS Omega. **7**, 8209 (2022); https://doi.org/10.1021/acsomega.2c00186
[11] https://oqmd.org/materials/structure/8413454
[12] https://oqmd.org/materials/structure/8430483
[13] A.Modwi, K.K.Taha, L.Khezami, Zeitschrift für PhysikalischeChemie **235**, 745 (2021); https://doi.org/10.1515/zpch-2019-1473
[14] https://en.wikipedia.org/wiki/Ultraviolet%E2%80%93visible_spectroscopy
[15]Unit-I Ultra-violet and Visible Spectroscopy, https://bbec.ac.in/wp-content/uploads/2015/08/Spectroscopy_UV-Visible.pdf
[16] 4.4:UV-Visible Spectroscopy - Chemistry LibreTexts. https://chem.libretexts.org/Bookshelves/Analytical_Chemistry/Physical_Methods_in_Chemistry_and_Nano_Science_%28Barron%29/04%3A_Chemical_Speciation/4.04%3A_UVVisible_Spectroscopy

[17] M. Tahenti, N Issaoui, T. Roisnel, S. Aleksandr, Kazachenko, A. Maximiliano, Iramain, Silvia Antonia Brandan, Omar Al-Dossary, A.S. Kazachenko, Houda Marouan, Zeitschrift für Physikalische Chemie **237**, 1775 (2023); https://doi.org/10.1515/zpch-2023-0332
[18] Y. Slimani, S.S. Meena, S.E. Shirsath, E. Hannachi, M.A. Almessiere, A. Baykal, R. Sivakumar, M. Khlid, Batoo, A. Thakur, I. Ercan, B. Özçelik, Zeitschrift für Physikalische Chemie **237**, 1753 (2023); https://doi.org/10.1515/zpch-2023-0215
[19] M. K. Halimah, M. F. Faznny, M. N. Azlan, H. A. A. Sidek, Results Phys. **7**, 581 (2017); https://doi.org/10.1016/j.rinp.2017.01.014
[20] H. Saudi, G. Adel, Optics **6**, 17 (2018)
[21] Gang Xiong, K. B. Ucer, R. T. Williams, U. Pal, J. Garcia Serrano, Phys. Stat. Solidi C **3**, 3577 (2006); https://doi.org/10.1002/pssc.200672164
[22] B. Rudraswamy, N. Dhananjaya, IOP Conf Series: Mater. Sci. Eng. **40**, 012034 (2012); https://doi.org/10.1088/1757-899X/40/1/012034
[23] A. T. M. Anishur Rahman, K. Vasilev, P. Majewski, J. Colloid Interface Sci. **354**, 592 (2011); https://doi.org/10.1016/j.jcis.2010.11.012
[24] R. K. Tamrakar, D. P. Bisen, K. Upadhyay, M. Sahu, I. P. Sahu, N. Bramhe, Superlattices Microstruct. **88**, 382 (2015); https://doi.org/10.1016/j.spmi.2015.09.033
[25] A. Dehelean, S. Rada, A. Popa, E. Culea, J. Mol. Struct. **1036**, 203 (2013); https://doi.org/10.1016/j.molstruc.2012.11.051
[26] M. Mazhdi, M. J. Tafreshi, Appl. Phys. A **124**, 863 (2018); https://doi.org/10.1007/s00339-018-2291-0
[27] M. W. Maswanganye, G. L. Kabongo, L. E. Mathevula, B. M. Mothudi, M. S. Dhlamini, Sci. Rep. **13**, 20131 (2023); https://doi.org/10.1038/s41598-023-47436-7
[28] Mehar Bhatnagar, Vishakha Kaushik, Akshey Kaushal, Mandeep Singh, Bodh Raj Mehta, AIP Adv. **6**, 095321 (2016); http://dx.doi.org/10.1063/1.4964313
[29] Mohan Jag, Organic Spectroscopy, Narosa Publication House, New Delhi, 2000.
[30] R.M. Silverstein, F.X. Webster, Spectrometric identification of organic compounds, John Wiley and Sons Inc, USA, 1991.
[31] K. Nakamoto, Infrared and Raman spectra of inorganic and coordination compounds, John Wiley & Sons, USA, 1986;
[32] https://terpconnect.umd.edu/~zhangx/html/ftir.html
[33] Santos T. Chartier , C. Pagnoux, J.F. Baumard, C.V. Santillii, S.H. Pulcinelli, A. Larbot, J. Eur. Ceram. Soc. **24**, 3713 (2004); https://doi.org/10.1016/j.jeurceramsoc.2004.03.003
[34] Rajendran Sorna Prema, Sengodan Kandasamy, J. Nanosci. **1**, 8348507 (2017); https://doi.org/10.1155/2017/8348507
[35]Sunday Wilson Balogun, Olusola Oladele James, Yekini Kolawole Sanusi, Oyeshola Hakeem Olayinka, SN Appl. Sci. **2**, 504 (2020); https://doi.org/10.1007/s42452-020-2127-3